

RESEARCH ARTICLE

Quantitative phosphoproteomic analysis provides insights into the aluminum-responsiveness of Tamba black soybean

Rongrong Han, Yunmin Wei, Yonghong Xie, Lusheng Liu, Caode Jiang*, Yongxiong Yu*

College of Animal Science and Technology, Southwest University, Beibei, Chongqing, China

* yuyongxiong8@126.com (YY); jcdpjax@swu.edu.cn (CJ)

OPEN ACCESS

Citation: Han R, Wei Y, Xie Y, Liu L, Jiang C, Yu Y (2020) Quantitative phosphoproteomic analysis provides insights into the aluminum-responsiveness of Tamba black soybean. PLoS ONE 15(8): e0237845. <https://doi.org/10.1371/journal.pone.0237845>

Editor: Tong Zhang, Pacific Northwest National Laboratory, UNITED STATES

Received: March 3, 2020

Accepted: August 4, 2020

Published: August 19, 2020

Copyright: © 2020 Han et al. This is an open access article distributed under the terms of the [Creative Commons Attribution License](https://creativecommons.org/licenses/by/4.0/), which permits unrestricted use, distribution, and reproduction in any medium, provided the original author and source are credited.

Data Availability Statement: All relevant data are within the paper and its Supporting Information files.

Funding: This work was supported by National Key R&D Program of China (No. 2018YFD0502000), State Cultivation Base of Eco-agriculture for Southwest Mountainous Land, and National Basic Research Program of China (No. 2014CB138701).

Competing interests: The authors have declared that no competing interests exist.

Abstract

Aluminum (Al^{3+}) toxicity is one of the most important limitations to agricultural production worldwide. The overall response of plants to Al^{3+} stress has been documented, but the contribution of protein phosphorylation to Al^{3+} detoxicity and tolerance in plants is unclear. Using a combination of tandem mass tag (TMT) labeling, immobilized metal affinity chromatography (IMAC) enrichment and liquid chromatography-tandem mass spectrometry (LC-MS/MS), Al^{3+} -induced phosphoproteomic changes in roots of Tamba black soybean (TBS) were investigated in this study. The Data collected in this study are available via ProteomeXchange with the identifier PXD019807. After the Al^{3+} treatment, 189 proteins harboring 278 phosphosites were significantly changed (fold change > 1.2 or < 0.83, $p < 0.05$), with 88 upregulated, 96 downregulated and 5 up-/downregulated. Enrichment and protein interaction analyses revealed that differentially phosphorylated proteins (DPPs) under the Al^{3+} treatment were mainly related to G-protein-mediated signaling, transcription and translation, transporters and carbohydrate metabolism. Particularly, DPPs associated with root growth inhibition or citric acid synthesis were identified. The results of this study provide novel insights into the molecular mechanisms of TBS post-translational modifications in response to Al^{3+} stress.

Introduction

Aluminum (Al^{3+}) stress poses a major constraint for plant productivity in acidic soils, which constitute approximately 50% of arable lands worldwide [1]. At $\text{pH} < 5.0$, soluble aluminum, which occurs mainly in the forms of Al^{3+} and $\text{Al}(\text{OH})^{2+}$, damages nuclei, reduces mitotic activity, inhibits root elongation and suppresses the absorption of water and nutrients [2–4]. The mechanisms underlying plant resistance to Al^{3+} have been the focus of recent research. An in-depth understanding of Al^{3+} -resistance mechanisms will favor the development of cultivated species suitable for acidic soils.

Plants in acidic soil have developed Al^{3+} exclusion and tolerance mechanisms. The exclusion mechanism prevents Al^{3+} from entering root cells via immobilizing Al^{3+} in the cell wall or by forming stable nonphytotoxic chelates with organic acid anions (OAs), such as citrate,

malate and oxalate, at the root apex [5, 6]. Internal tolerance mechanisms enable root cells to sequester Al^{3+} in vacuoles [7]. For decades, a number of proteins contributing to Al^{3+} tolerance have been identified in plants, and many studies have provided direct evidence linking Al^{3+} -induced OA exudation from plant roots to malate and citrate efflux transporters (ALMTs), multidrug and toxic compound extrusion proteins (MATEs) and H^+ -ATPase activity in the plasma membrane [1, 8]. In *Stylosanthes* roots, our recent data revealed that the signaling cascades of Al^{3+} -induced citrate exudation comprise heterotrimeric G-proteins, phosphoinositide phospholipase C (PLC), inositol triphosphate (IP_3), diacylglycerol (DAG), Ca^{2+} and protein kinases [9].

Protein phosphorylation, which is one of the most important post-translational protein modifications, can modulate the functions of proteins. Salicylic acid (SA) can mitigate Al^{3+} toxicity by affecting a signaling pathway associated with protein phosphorylation in *Coffea arabica* L. suspension cells [10]. Importantly, OA transport proteins in response to Al^{3+} are post-translationally regulated by protein phosphorylation. In wheat (*Triticum aestivum*), Al^{3+} -induced malate efflux as effectively blocked by K-252a, which is a broad range inhibitor of protein kinases [8]. Plasma membrane H^+ -ATPase was hyperphosphorylated after Al^{3+} treatment at a concentration below 50 μM in soybean (*Glycine max*) roots [11]. Our previous research also demonstrated that phosphorylation is responsible for the interaction of H^+ -ATPase and 14-3-3 protein, which leads to Al^{3+} -stimulated citrate exudation in roots of Tamba black soybean (*Glycine max* cv. Tamba, TBS) [12–14]. Additionally, genome-wide association analysis [15], transcriptomics [9, 16] and proteomics [17] have allowed the exploration of the mechanisms of Al^{3+} resistance globally. However, phosphorylated proteins related to Al^{3+} -induced citrate exudation at the global scale have rarely been reported.

In recent years, quantitative phosphoproteomics using tandem mass tag (TMT) labeling has provided useful information for subsequent functional studies, and has been applied to examinations of plant phosphorylated proteins during abiotic and biotic stress [18, 19] and during plant growth and development [20]. Hence, this approach was employed to evaluate differentially regulated phosphoproteins induced by Al^{3+} stress in roots of the Al^{3+} -resistant cultivar TBS. The identified Al^{3+} -induced phosphoproteins can enable further investigation of the Al^{3+} tolerance mechanisms related to citrate secretion from roots of TBS plants.

Materials and methods

Cultivation of TBS plants

TBS seeds were disinfected with 1% sodium hypochlorite for 20 min and washed in double-distilled water three times. The seeds were incubated on moistened filter papers at 25°C. After germination, the seedlings were transplanted into 8 L aquariums containing 1/2 Hoagland's nutrient solution (pH 6.0), which was renewed every two days. The seedlings were grown in an artificially lit room at 27°C/22°C (day/night) with 14 h of light (200 $\mu\text{mol}/\text{m}^2/\text{s}$) for 2 weeks.

Al^{3+} treatment and measurement of the relative root growth (RRG), citrate content and citrate secretion

For treatment, uniform seedlings were pre-grown overnight in a 0.5 mM CaCl_2 solution (pH 4.5) at 25°C under constant light as described above. Then, every ten seedlings were transferred into solutions containing 0 (control) or 50 μM AlCl_3 (both containing 0.5 mM CaCl_2 , pH = 4.5) for 72 h according to previous studies with minor modifications [21]. The harvested root tips were stored in a -80°C freezer after snap-freezing in liquid nitrogen for future use.

For phosphoproteomic analysis, there were three replicates per treatment, namely, 0 μM (1), 0 μM (2), and 0 μM (3) for the control groups, and 50 μM (1), 50 μM (2), and 50 μM (3) for the Al^{3+} -treatment groups.

For the measurement of RRG, TBS plants were transferred into a 0 (control) or 50 μM AlCl_3 solution (both containing 0.5 mM CaCl_2 , pH = 4.5) for 24, 48 and 72 h, respectively. Root length was measured before and after treatment. RRG analysis was carried out according to the procedures described by Min [13]. The analysis was performed with three replicates with 5 plants per replicate.

For the measurement of the citrate content and citrate secretion, TBS plants were transferred into 0 and 50 μM AlCl_3 solutions (containing 0.5 mM CaCl_2 , pH = 4.5), and the roots and root exudates were collected at 3, 6, 12, 24, 48 and 72 h. Then, 0.1 g root tips was ground in 1 mL ddH₂O and centrifuged at 12,000 rpm for supernatant collection. The citrate content was measured by enzymic determination according to Zhao [22]. There were three replicates for each time point with 5 plants per replicate.

Protein extraction, digestion, TMT labeling and phosphopeptide enrichment

Proteins extraction was carried out according to the procedures described by Sun [18] with slight modification. The protein concentration was evaluated with the BCA kit (Beyotime, Shanghai, China). For protein digestion, trypsin (Promega, Wisconsin, USA) was added at a 1:50 trypsin-to-protein mass ratio for overnight digestion and at a 1:100 trypsin-to-protein mass ratio for another 4 h digestion. After the digested solutions were desalted with a Strata X C18 SPE column (Phenomenex, California, USA) and vacuum-dried, they were dissolved in 0.5 M TEAB, and labeled as 0 μM (3)-126, 0 μM (2)-127, 0 μM (1)-128, 50 μM (3)-129, 50 μM (2)-130, and 50 μM (1)-131 using a TMT kit (Thermo Scientific, Waltham, USA). The TMT-labeled peptides were separated into 60 fractions with a gradient of 8 to 32% acetonitrile (pH 9.0) over 60 min. The collected peptides were recombined into 8 fractions and dried via vacuum centrifugation.

For phosphopeptides enrichment, the peptides in each fraction were incubated under gentle vibration in an immobilized metal affinity chromatography (IMAC) microsphere suspension in loading buffer (50% acetonitrile/6% trifluoroacetic acid). The phosphopeptides absorbed by the IMAC microspheres were collected by centrifugation and were washed with 50% acetonitrile plus 6% trifluoroacetic acid and with 30% acetonitrile plus 0.1% trifluoroacetic acid. The enriched phosphopeptides were eluted with 10% NH_4OH and then lyophilized for liquid chromatography-tandem mass spectrometry (LC-MS/MS) analysis.

LC-MS/MS and MS/MS data analysis

The peptides were dissolved in solvent A (0.1% formic acid) and separated with a gradient according to the following procedure, i.e., 6 to 23% solvent B (0.1% formic acid in 98% acetonitrile) over 26 min, 23 to 35% solvent B for 8 min, and 80% solvent B for 6 min. The tryptic peptides were separated using an EASY-nLC 1000 UPLC system at a constant flow rate of 400 nL/min and then subjected to ionization using an NSI source, followed by tandem mass spectrometry (MS/MS) analysis in Q ExactiveTM Plus (Thermo Scientific, Waltham, USA) online-coupled to the UPLC. The electrospray voltage applied was 2.0 kV. A full mass scan over the range of m/z 350 to 1800 was obtained with a resolution of 70000, while the fragments were detected in the Orbitrap at a resolution of 17,500 at m/z 100. For MS/MS, the normalized collision energy (NCE) was set to 28%, the dynamic exclusion time of the MS/MS scanning was set to 15 s, and the automatic gain control (AGC) was set at 5E4.

The Maxquant search engine (v.1.5.2.8) was applied to process the MS/MS data according to Chen's work [23]. Tandem mass spectra of peptides were searched against the Phytozome 12.1-*Glycine max* Wm82.a2.v1 database concatenated with the reverse decoy database. The false discovery rate (FDR) was adjusted to $< 1\%$ and the minimum score for modified peptides was > 40 . The number of unique peptides was set to ≥ 2 .

Bioinformatics methods

Functional annotation of differentially phosphorylated proteins (DPPs) was performed using the Uniprot-GoA database (<http://www.ebi.ac.uk/GOA/>) for GO annotation. The Kyoto Encyclopedia of Genes and Genomes (KEGG) online service tools (<https://www.kegg.jp/kegg/>) were used to perform KEGG pathway mapping of the annotated protein KEGG database descriptions. Only categories with a two-tailed Fisher's corrected p -value < 0.05 were considered to indicate a significant enrichment of DPPs against all identified proteins. The updated version of WOLFPSORT (<http://www.genscript.com/wolf-psort.html>) was used to predict subcellular localizations. Soft motif-X was applied to analyze the phosphorylation motifs at specific positions of modified-13-mers (6 amino acids upstream and downstream of the site) in the whole protein sequences. The significance threshold was set to $p < 10^{-6}$, and the minimum occurrence of motifs was set to 20. Protein-protein interactions (PPIs) were analyzed by the Search Tool for the Retrieval of Interaction Genes/Proteins (STRING) database (<http://string-db.org/>). The interaction confidence score was set at a high level (≥ 0.7). The interaction network from STRING was visualized in Cytoscape (<http://www.cytoscape.org/>). The thresholds used for the identification of significant DPPs were set at a fold change > 1.2 or < 0.83 and $p < 0.05$.

Statistical analysis

Data for the root growth, citrate content and secretion are presented as the mean \pm the standard error of the mean (SEM). One-way ANOVA followed by Duncan's test was used to compare significance among treatments. Statistical significance was set to $p < 0.05$. SPSS Statistics19 and GraphPad (Version 8.3.0) were used for statistical analysis and graph preparation, respectively.

Results

Effect of the Al^{3+} treatment on the RRG, citrate content and secretion in TBS roots

Under Al^{3+} stress, root elongation of the plants was inhibited. The RRG of TBS was reduced by $> 50\%$ within 24, 48 and 72 h after the Al^{3+} treatment ($p < 0.05$) (Fig 1A). The Al^{3+} treatment significantly decreased the citrate content in the root tips within 3, 6, 12, 24, 48 and 72 h ($p < 0.05$) (Fig 1B), while citrate secretion from the root tips was significantly increased ($p < 0.05$) (Fig 1C). These results are similar to those of Eticha's research [24].

Analyses of phosphorylated proteins and sites in TBS roots under Al^{3+} stress

The phosphoproteomic profiles were evaluated in root tips of TBS seedlings after the Al^{3+} treatment for 72 h. The mass spectrometry proteomics data have been deposited to the ProteomeXchange Consortium via the PRIDE partner repository with the dataset identifier PXD019807 (Username: reviewer89780@ebi.ac.uk, Password: NKBxNBA3). In total, 6156 phosphopeptides representing 1415 proteins were obtained, among which 3245 phosphosites

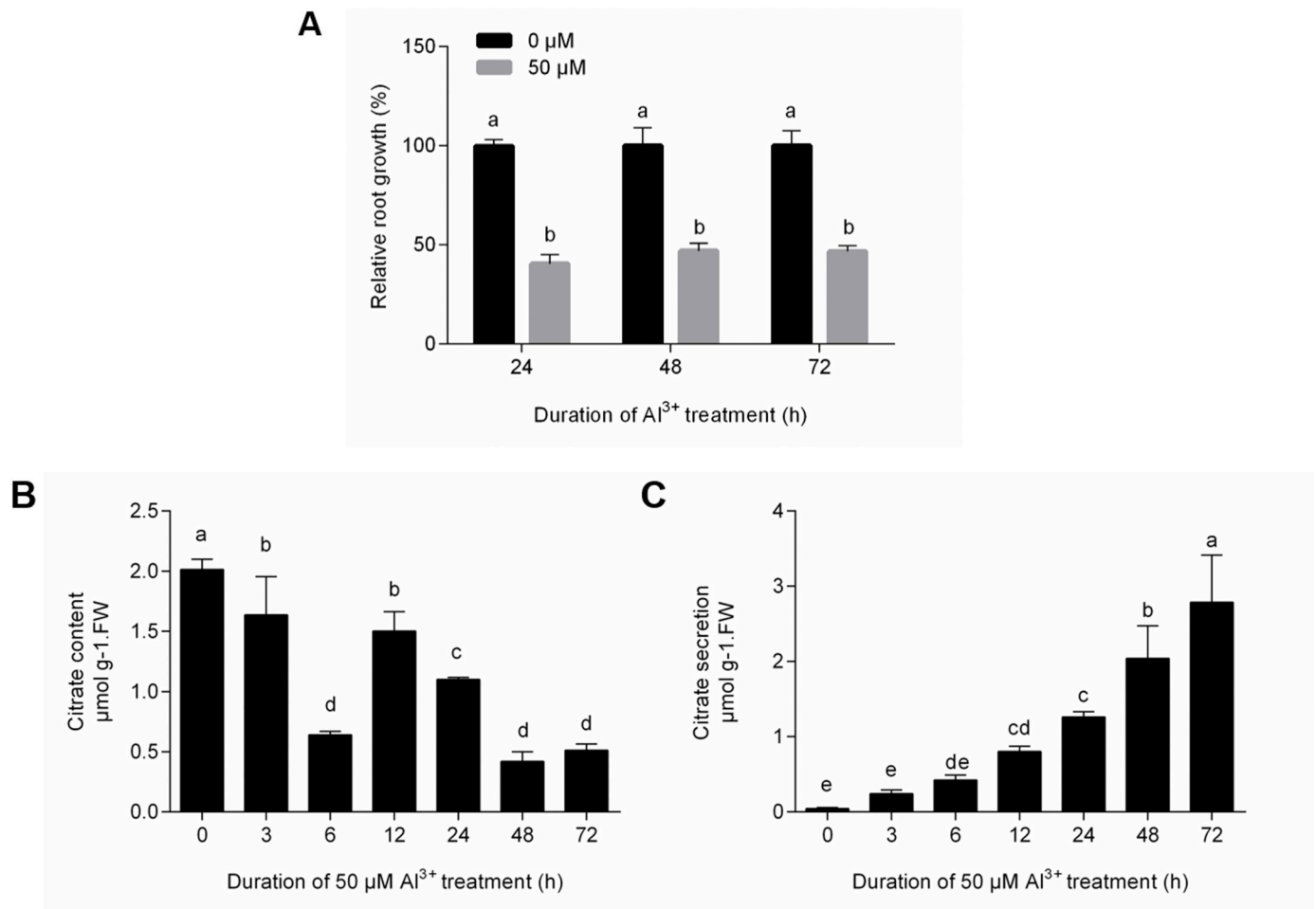


Fig 1. Effect of the Al³⁺ treatment on TBS roots. (A) Relative root growth; (B) Citrate content; (C) Citrate secretion. The bars are the means \pm standard deviation of three replicates. Different letters above columns indicate significance (Duncan, $p < 0.05$).

<https://doi.org/10.1371/journal.pone.0237845.g001>

from 1280 proteins provided quantitative information (S1 Table). The peptide mass error was distributed mainly between -5 and 5 ppm (S1A Fig). Approximately 29.96% of the peptides were phosphorylated at a single site, while phosphopeptides with two, three or four sites constituted 28.48, 17.81 and 7.62% of the total, respectively (S1B Fig). Additionally, the lengths of more than 95.42% peptides were distributed between 7 and 21 amino acids (aa), consistent with the properties of tryptic peptides.

DPPs in response to the Al³⁺ treatment

The DPPs in roots between the Al³⁺-treated (50 μM) and non-treated control groups (0 μM) were examined. A total of 189 phosphoproteins, including 88 upregulated in regard to phosphorylation (> 1.2 -fold, $p < 0.05$), which possessed 135 phosphorylation sites, and 96 downregulated in regard to phosphorylation containing 131 phosphorylation sites (< 0.83 -fold, $p < 0.05$), were differently phosphorylated under Al³⁺ stress (Fig 2A, S2 Table). In addition, 5 DPPs contained both upregulated (6) and downregulated (6) phosphorylation sites. Of all the phosphorylation sites in the DPPs, 85.97% were serine phosphorylation, and threonine and tyrosine phosphorylation represented 10.43 and 3.60%, respectively (Fig 2B, S2 Table).

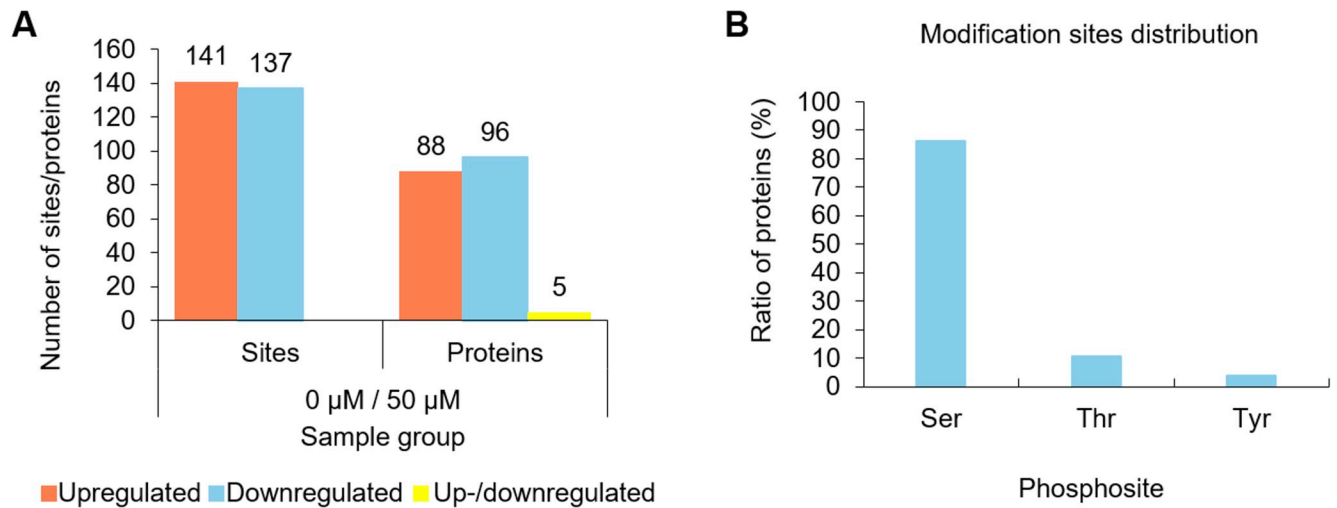


Fig 2. Distribution of phosphorylated proteins and phosphorylated sites. (A) The number of up-, down-, and up-/downregulated phosphorylated sites and proteins in the root of Al^{3+} -treated (50 μM) and untreated (0 μM) plants. (B) Distribution of phosphorylation sites at serine, threonine and tyrosine residues. Three biological replicates were performed.

<https://doi.org/10.1371/journal.pone.0237845.g002>

Functional classification of the DPPs

The DPPs were annotated using gene ontology (GO) terms based on biological processes (BP), cellular components (CC), and molecular functions (MF). For the BP category, the DPPs were classified into metabolic processes, cellular processes, single-organism processes, localization, cellular component organization or biogenesis, and other (S2A Fig). In the CC category, the DPPs were grouped into cell processes, organelle processes, macromolecular complex processes, and membrane processes (S2B Fig). Regarding the MF category, the DPPs belonged to the categories of binding, catalytic activity, molecular function regulator, transporter activity, and other (S2C Fig).

The subcellular localization of the DPPs was further analyzed. Most of the DPPs were located in the nucleus, chloroplast, cytoplasm and plasma membrane (S3A Fig). While 56% of the upregulated phosphoproteins were located in the nucleus, 19 and 13% were located in the chloroplast and cytoplasm, respectively (S3B Fig). Of the downregulated phosphoproteins, 66% were located in the nucleus, whereas 11, 9 and 8% were located in the chloroplast, cytoplasm, and plasma membrane, respectively (S3C Fig).

Enrichment analysis of the DPPs under Al^{3+} -treatment

GO enrichment analysis according to CC terms showed that the upregulated DPPs were over-represented in the cytoplasmic part, while the DPPs were downregulated in the membrane-bounded organelle (S4 Fig, S3 Table). In terms of the MF, the enriched terms in the upregulated DPPs were related to enzyme regulator activity, hydrolase activity (acting on glycosyl bonds), GTPase regulator activity, nucleoside-triphosphatase regulator activity, GTPase activator activity, enzyme activator activity, and O-acyltransferase activity, whereas the downregulated DPPs were associated with histone binding, RNA binding, signal transducer activity, translation initiation factor activity, and nucleic acid binding. The BP terms dominant for upregulated DPPs included the processes of glycerolipid metabolism, protein modification, cellular protein modification, and phosphorylation, but the downregulated DPPs were enriched in the processes of RNA metabolism and nucleic acid metabolism. These results

indicated that the DPPs were related to stress, homeostasis, amino acid metabolism, transport processes and energy metabolic processes.

KEGG enrichment analysis revealed that all the DPPs were enriched in three categories, namely, spliceosome, mRNA surveillance and RNA transport (S4 Table). The upregulated DPPs were involved in RNA degradation and endocytosis pathways (S5A Fig, S4 Table). The downregulated DPPs were associated with spliceosome, RNA transport, and the mRNA surveillance pathway (S5B Fig, S4 Table). These results were consistent with the results of the GO terms, indicating that the DPPs were distributed to transport and RNA replication and modification.

The motifs were analyzed with the motif-X algorithm for the phosphorylation sites from the -6 to 6 positions in the DPPs. In all the phosphoproteins, 55 phosphorylation motifs were identified ($8.71 \leq \text{motif score} \leq 43.05$, S5 Table). The motifs distributed in the DPPs are listed in the S6 Table.

PPI of phosphoproteins

Usually, proteins take part in diverse cellular processes via forming a complex regulatory network. To reveal the functional relationships among the DPPs, the PPI network was constructed using STRING version 10.0 and a confidence score of ≥ 0.7 (high confidence). As shown in Fig 3, the PPI network was involved in spliceosome (A), membrane trafficking (B), carbohydrate metabolism (C), ribosome biogenesis in eukaryotes (D), and signal transduction (E). The detailed information of the nodes is listed in S7 Table.

DPPs involved in signal transduction

Seventeen DPPs involved in cell signaling were increased, while 5 DPPs were decreased in phosphorylation under the Al^{3+} treatment (Table 1, S2 and S8 Tables). These DPPs were associated with serine/threonine kinases (9), diacylglycerol and inositol metabolism (3), the ras family (4), kinase cascades (3) and others (3). Among serine/threonine kinases, BLUS1 (Glyma.10G173000.5.p, Glyma.20G217200.2.p), EDR1 (Glyma.12G128700.3.p), HT1 (Glyma.13G238400.7.p), and DDB (Glyma.15G261200.4.p) were observed to be hyperphosphorylated under Al^{3+} stress, while PRPF4B (Glyma.05G011400.3.p) and PBS1 (Glyma.13G289900.2.p) were hypophosphorylated. For diacylglycerol and inositol metabolism, 2 diacylglycerol acyltransferase (Glyma.07G036400.1.p and Glyma.09G065300.2.p) and 1 phosphatidylinositol 4-phosphate 5-kinase 7 (Glyma.08G186400.3.p) were determined to be upregulated in regard to phosphorylation. Additionally, 4 ADP-ribosylation factor GTPase-activating proteins (Glyma.08G039600.1.p, Glyma.08G271700.1.p, Glyma.09G188300.2.p and Glyma.19G172700.1.p) belonging to the ras family were all hyperphosphorylated by Al^{3+} . Regarding kinase cascades, CPK1 (Glyma.10G120300.2.p) and CKI (Glyma.13G105900.2.p) were hyperphosphorylated, while MAPK (Glyma.18G236800.2.p) was hypophosphorylated.

DPPs involved in transcription, translation and post-translational modification

Twenty DPPs, associated with transcription factors (TFs) and translation and post-translational modification, were examined under Al^{3+} stress (Table 1, S2 and S9 Tables). For the TFs, Al^{3+} enhanced the phosphorylation of the zinc finger protein GIS2 (Glyma.04G008700.1.p) and MYB183 (Glyma.06G187600.1.p), while it suppressed the phosphorylation of GT-2 (Glyma.06G149900.2.p) and bZIP56 (Glyma.18G283800.2.p). Additionally, 1 transcriptional coactivator (Glyma.06G155900.1.p) was hypophosphorylated under Al^{3+} stress.

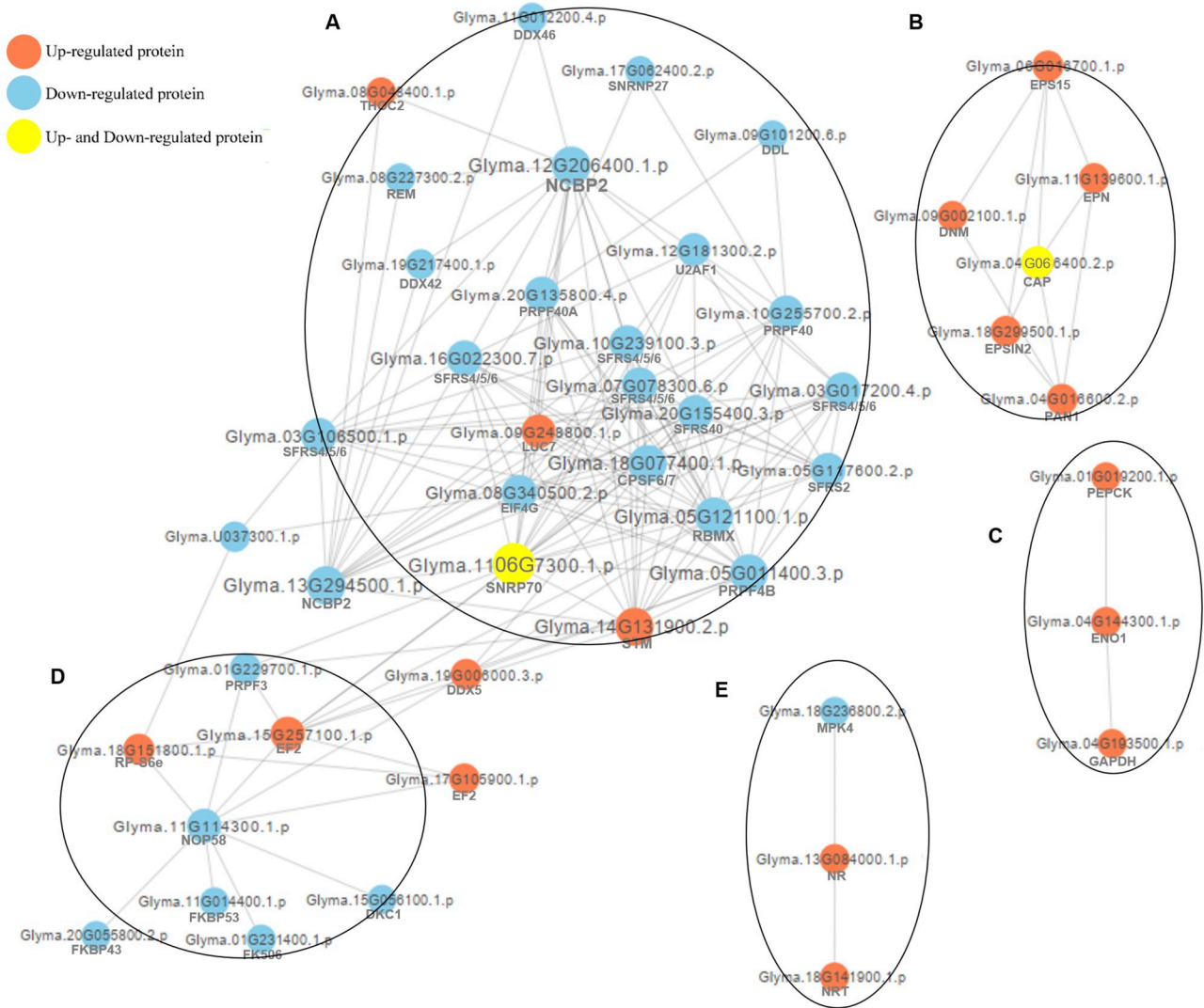


Fig 3. Protein-protein interaction networks of differentially phosphorylated proteins (DPPs) under Al³⁺ treatment in TBS seedlings. (A) Spliceosome; (B) Membrane trafficking; (C) Carbohydrate metabolism; (D) Ribosome biogenesis in eukaryotes; (E) Signal transduction.

<https://doi.org/10.1371/journal.pone.0237845.g003>

For translation, eukaryotic translation initiation factors (EIF) (Glyma.03G106500.1.p, Glyma.08G340500.2.p and Glyma.U037300.1.p) were hypophosphorylated by Al³⁺, while EIF 4B2 was upregulated and downregulated at Ser₅₁₀ and Ser₅₀₁, respectively. Peptidyl-prolyl cis-trans isomerases, which allow proteins to fold into their correct conformations, were hypophosphorylated by Al³⁺, including CYP63 (Glyma.03G157900.2.p) and FKBP53 (Glyma.01G231400.1.p, Glyma.11G014400.1.p and Glyma.20G055800.2.p). In addition, Al³⁺ upregulated the phosphorylation of the ribosomal proteins S6 and S11. Regarding post-translational modifications, 4 E3 ubiquitin-protein ligases were found, with ATL6 (Glyma.10G156500.1.p), LIN1 (Glyma.10G194500.2.p) and MARCH7 (Glyma.13G139200.3.p) upregulated, and RBBP6 (Glyma.17G143300.2.p) downregulated.

Table 1. Summary of the phosphoproteins affected by Al³⁺.

Protein category	Total	Upregulated	Downregulated	Up-/downregulated
Signal transduction	22	17	5	0
Transcription	5	2	3	0
Translation and post-translational modification	15	6	8	1
Carbohydrate metabolism	10	10	0	0
Transporter	8	6	2	0
Membrane trafficking	8	5	2	1
DNA and RNA processing/modification	30	11	19	0
Cytoskeleton	15	4	10	1
Miscellaneous	37	12	24	1
Uncharacterized protein	39	15	23	1

<https://doi.org/10.1371/journal.pone.0237845.t001>

DPPs involved in carbohydrate metabolism

The Al³⁺-induced release of citrate plays an important role in Al³⁺ resistance in soybean [25]. The synthesis of citric acid occurs in the tricarboxylic cycle (TCA), which plays an important role in carbon metabolism. In total, 10 DPPs involved in carbohydrate metabolism were significantly increased in response to Al³⁺ stress (Table 1, S2 and S10 Tables). Among the DPPs involved in the TCA, aconitate hydratase (ACO) (Glyma.01G162800.1.p) was hyperphosphorylated (Fig 4). Regarding glycolysis and gluconeogenesis, phosphorylation of glyceraldehyde-3-phosphate dehydrogenase (GAPDH, Glyma.04G193500.1.p) and phosphoenolpyruvate carboxykinase (PEPCK, Glyma.01G019200.1.p) was observed to be upregulated, respectively (Fig 4). For sucrose metabolism, sucrose synthase (SUS, Glyma.15G182600.2.p) was found to be hyperphosphorylated (Fig 4). In the oxalate cycle, oxalate-CoA ligase (OCL, Glyma.11G198300.1.p) was hyperphosphorylated by more than 2-fold by Al³⁺.

DPPs involved in transporters

Transporters are critical for the alleviation of Al³⁺-induced root growth inhibition [26], Al³⁺-induced secretion of OAs [27] and Al³⁺ uptake, sequestration and distribution [7]. In total, 8 transporters were identified (Table 1, S2 and S11 Tables). Among them, 6 DPPs were increased, while 2 DPPs were decreased in regard to phosphorylation. The upregulated DPPs belonged to amino acid transporters (2 lysine histidine transporters, Glyma.01G161100.1.p and Glyma.11G082700.1.p), the ABC transporter family (1 ABC transporter, Glyma.13G119000.2.p), inorganic ion transporters (1 potassium transporter, Glyma.19G263100.1.p and 1 high affinity nitrate transporter, Glyma.18G141900.1.p), etc. The downregulated DPPs belonged to amino acid transporters (1 lysine histidine transporter, Glyma.15G068700.2.p) and inorganic ion transporters (1 boron transporter 1, Glyma.03G222300.1.p).

Discussion

To the best of our knowledge, this study represents one of the first quantitative phosphoproteomic analyses characterizing responses to Al³⁺ in TBS seedlings. The findings showing that the Al³⁺ treatment inhibited root growth, reduced the root citrate content and increased root citrate secretion (Fig 1) make it possible to analyze Al³⁺-response proteins in TBS. We believe that the significant decrease of the citrate content of root tips after the Al³⁺ treatment was related to the enhanced citrate exudation. The error rate and length distribution of the enriched peptides, which are consistent with the properties of tryptic peptides, indicate the accuracy of the mass spectrometry data (S1 Fig). Particularly, the identified phosphorylation

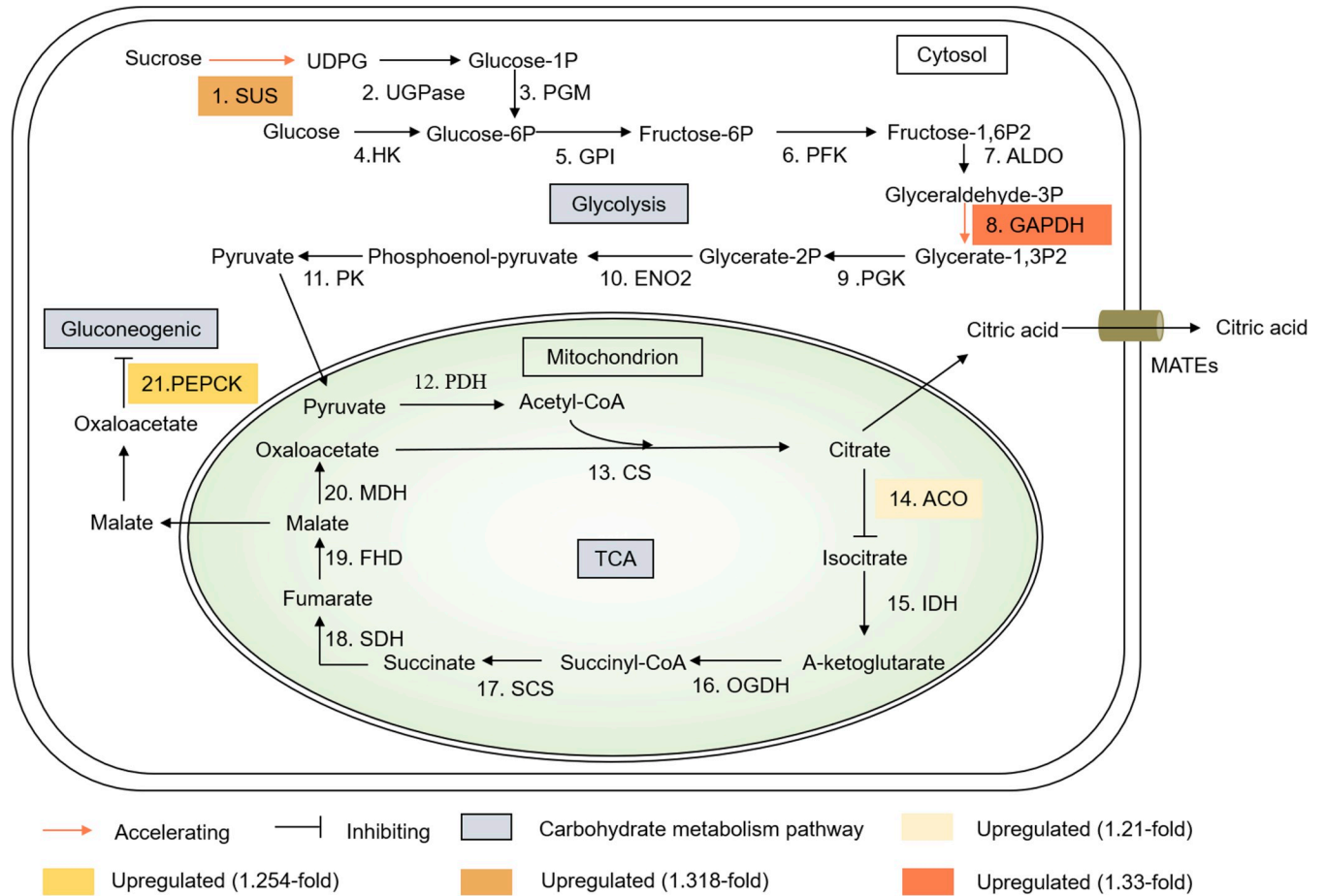


Fig 4. DPPs involved in carbohydrate metabolism. 1. SUS, sucrose synthase; 2. UGPase, UDP-glucose pyrophosphorylase; 3. PGM, phosphoglucomutase; 4. HK, hexokinase; 5. GPI, glucose-6-phosphate isomerase; 6. PFK, phosphofructokinase; 7. ALDO, aldolase; 8. GAPDH, glyceraldehyde-3-phosphate dehydrogenase; 9. PGK, phosphoglycerate kinase; 10. ENO2, enolase2; 11. PK, pyruvate kinase; 12. PDH, pyruvate dehydrogenase; 13. CS, citrate synthase; 14. ACO, aconitate hydratase; 15. IDH, isocitrate dehydrogenase; 16. OGDH, α -ketoglutarate dehydrogenase complex; 17. SCS, succinyl-CoA synthetase; 18. SDH, succinate dehydrogenase; 19. FHD, fumarase; 20. MDH, malate dehydrogenase; 21. PEPCK, phosphoenolpyruvate carboxykinase.

<https://doi.org/10.1371/journal.pone.0237845.g004>

sites and DPPs in response to Al^{3+} stress provide a rich source for use in investigating the multiple mechanisms underlying Al^{3+} tolerance in TBS.

Global analysis of DPPs under Al^{3+} stress

Inhibition of root elongation can be easily observed under Al^{3+} stress [28]. However, TBS root released citrate to relieve toxicity [14]. In our work, most of the DPPs associated with spliceosome and ribosome biogenesis in eukaryotes (Fig 3) were hypophosphorylated, and hyperphosphorylated DPPs of membrane trafficking might contribute to the inhibition of root growth [29–31]. On the other hand, the majority of the DPPs categorized as belonging to signal transduction and carbohydrate metabolism (Fig 3) underwent hyperphosphorylation, which was conducive to Al^{3+} -induced signal transduction and citric acid synthesis and release against Al^{3+} toxicity.

DPPs involved in signal transduction

Our recent data established that Al^{3+} sensing in *Stylosanthes* requires the G-protein-mediated signaling pathway, which includes PLC, phosphatidylinositol 4, 5-phosphate (PIP2), IP3,

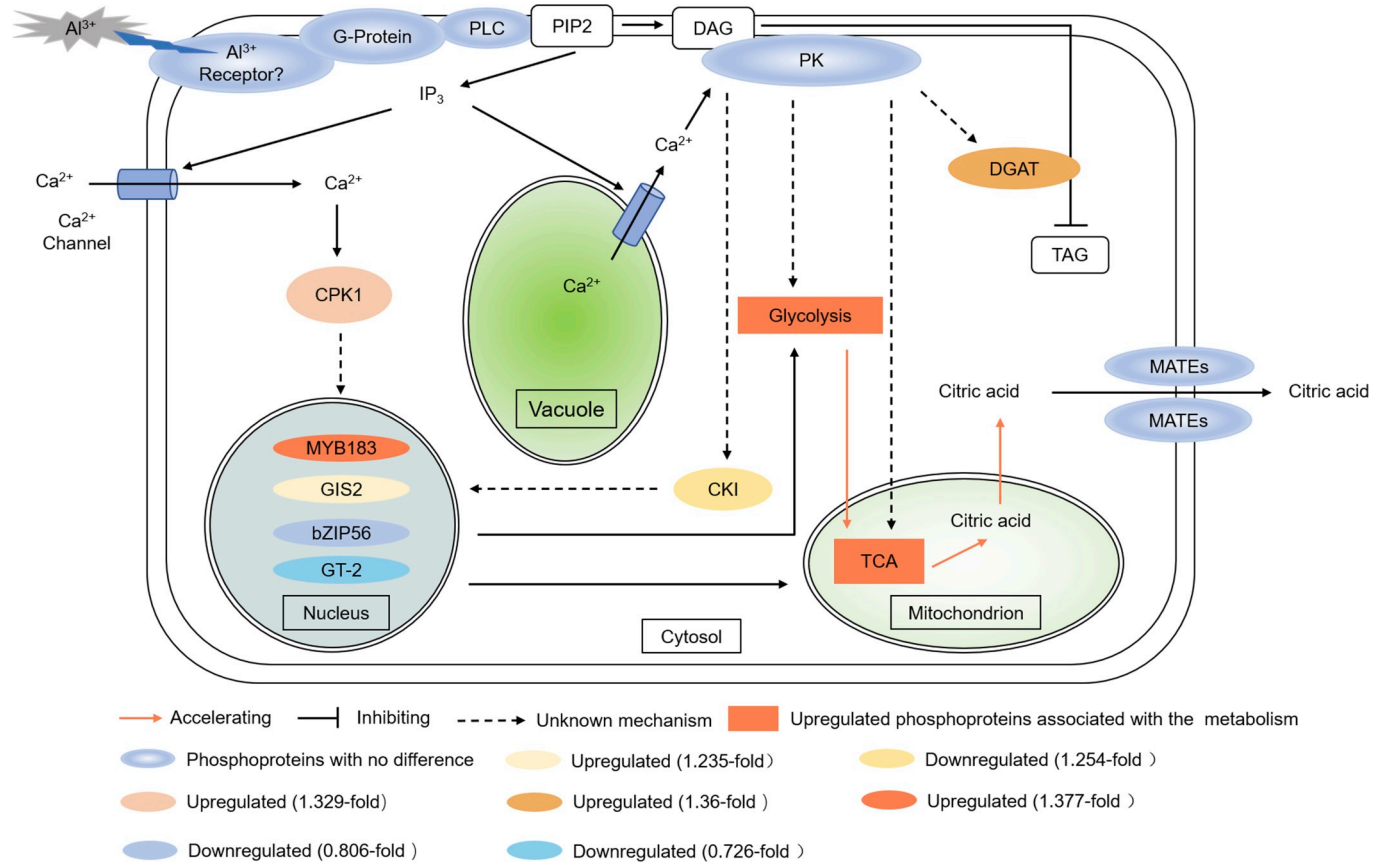


Fig 5. Putative model illustrating the signaling cascades of the Al³⁺-induced exudation of citrate from TBS roots. Phosphoinositide phospholipase C (PLC), phosphatidylinositol 4, 5-phosphate (PIP2), diacylglycerol (DAG), diacylglycerol acyltransferases (DGAT), triacylglycerol (TAG), protein kinases (PK), inositol triphosphate (IP3), calcium-dependent protein kinase (CPK), transcription factor (TF), casein kinase I (CKI), tricarboxylic acid (TCA).

<https://doi.org/10.1371/journal.pone.0237845.g005>

DAG, Ca²⁺ and protein kinases [9]. Proteins associated with the G-protein-mediated signaling pathway, DGAT and kinase cascades (CPK1 and CKI) were detected in the present study (S1, S2 and S8 Tables). The activity of DGAT was inhibited by phosphorylation [32]. Therefore, hyperphosphorylation of DGAT promoted signal transduction via DAG accumulation under Al³⁺ stress. Furthermore, phosphorylation of CPK1 and CKI was enhanced by the Al³⁺ treatment (Fig 5, S2 and S8 Tables). Actually, CPKs have been reported to phosphorylate target proteins, such as transcription factors (TFs), to specify the reprogramming of genes [33]. SeCKI has been reported to regulate *SeFAD2* expression via phosphorylation of the SebHLH transcription factor [34]. Taken together, the results show that the Al³⁺ tolerance of soybean involves phosphorylation in G-protein-mediated Al³⁺ signaling and kinase cascades.

DPPs involved in transcription

Evidence shows that transcription factors such as the MYB [16], WRKY [35], zinc finger protein [27], MADS-box [36], NAC [37, 38] and bZIP [39] families are required for Al³⁺ responses. In our work, the zinc finger protein GIS2 and MYB183 were hyperphosphorylated under Al³⁺ stress, while bZIP56 and GT-2 were hypophosphorylated (Fig 5, S2 and S9 Tables). Soybean tolerance to salinity was enhanced by inoculation with rhizobia via inhibiting the phosphorylation of GmMYB183 and inhibiting its activity in *GmCYP81E11* expression transcriptional regulation [40]. However, GmMYB183 was hyperphosphorylated at Ser₃₆ in

response to Al^{3+} stress. This might be due to GmMYB183 being phosphorylated by different kinases in response to different stimuli. In *Arabidopsis*, the phosphorylation of MYB41 and the zinc finger transcriptional regulator ZAT6 were required for the tolerance of salt during seed germination and root growth [41, 42]. Phosphorylated MYB15 promotes *CBF3* expression, which regulates root growth under freezing stress, via reducing its binding to the *CBF3* promoter [43, 44]. The phosphorylation of *AREB1*, which is a bZIP, is required for the expression of ABA-inducible genes [45]. *STOPI*, which is a Cys2/His2 type zinc-finger protein, regulates the expression of Al^{3+} -resistance genes in *Arabidopsis*, and the phosphorylation of *STOPI* enhances malate exudation under Al^{3+} stress [46]. Therefore, we speculated that the TFs, detected in our work, regulated the expression of genes associated with root growth and citric acid synthesis based on phosphorylation or dephosphorylation.

DPPs promotes citric acid synthesis under Al^{3+} stress

It has been recognized that Al^{3+} tolerance in beans relies on their capacity for citric acid synthesis, which is related to carbohydrate metabolism [24]. The DPPs, associated with carbohydrate metabolism, were all hyperphosphorylated in this work (S2 and S10 Tables). In higher plants, sucrose, as the main form of carbohydrate transport, can be digested into glucose, contributing to glycolysis. *SUS*, which is activated by phosphorylation [47], converts sucrose into glucose-6P, which plays a role in the glycolytic pathway. In the present study, hyperphosphorylated *SUS* promoted the glycolytic pathway under Al^{3+} stress (Fig 4). Meanwhile, *GAPDH*, which is an enzyme involved in glycolysis, was shown to be hyperphosphorylated after the Al^{3+} treatment (Fig 4). The enzyme was activated by phosphorylation [48], and then, Al^{3+} stress accelerated the glycolytic rate.

Citric acid metabolism, as part of the tricarboxylic acid (TCA) cycle, occurs in mitochondria. Our data revealed that *ACO* was hyperphosphorylated in response to Al^{3+} stress (Fig 4). *ACO*, which is an enzyme that catalyzes the transformation of citric acid into isocitrate in the TCA cycle, was downregulated by exogenous SA under Al^{3+} stress enhancing citrate release from soybean roots [49]. *ACO* was detected to be hyperphosphorylated in TBS roots under Al^{3+} stress, and we speculated that the phosphorylation of *ACO* weakened its activity and increased the accumulation of citric acid.

In addition, hyperphosphorylated *PEPCK* was found in our study (Fig 4). It has been reported that *PEPCK* activation is suppressed by phosphorylation [50, 51]. Hence, the activation-suppressed *PEPCK* results in an accumulation of oxaloacetate, contributing to citric acid synthesis. Overall, the phosphorylation of proteins linking carbohydrate metabolism pathways facilitates citric acid synthesis for Al^{3+} detoxification in TBS roots.

Conclusions

This study explored the mechanism of Al^{3+} resistance through global phosphorylation levels in TBS plants. According to the results, 189 of 1280 quantified proteins were significantly differentially phosphorylated in response to Al^{3+} stress. Among them, 88 DPPs were upregulated, 96 DPPs were downregulated, and 5 DPPs were both up-/downregulated in regard to phosphorylation. Functional analysis of DPPs, together with PPI analysis, revealed DPPs associated with the inhibition of root growth and citric acid synthesis metabolism. Of these, the DPPs of the Al^{3+} signaling cascades comprised *CPK1*, *CKI* and *DGAT*, and those of the citric acid synthesis metabolism included *SUS*, *GAPDH*, *ACO* and *PEPCK*. As a consequence, our work provides important data for understanding the Al^{3+} signaling and enhanced citric acid synthesis metabolism in response to Al^{3+} stress in TBS plants.

Supporting information

S1 Fig. Quality control validation of mass spectrometry data. (A) Volcano map of the error rate distribution for mass spectrometry; (B) Length distribution of the phosphorylated peptides.

(TIF)

S2 Fig. GO function classifications of differentially phosphorylated proteins (DPPs) in Al³⁺-treated plants compared with untreated controls. (A) Biological process; (B) Cellular component; (C) Molecular function.

(TIF)

S3 Fig. Subcellular localization prediction of DPPs in Al³⁺-treated plants compared with untreated controls. (A) All DPPs; (B) Upregulated DPPs; (C) Downregulated DPPs.

(TIF)

S4 Fig. Gene ontology (GO) enrichment analysis of DPPs according to cellular components, molecular functions and biological processes.

(TIF)

S5 Fig. KEGG pathway enrichment analysis of the 50 μM versus 0 μM Al³⁺ treatments. Enriched KEGG pathways for upregulated proteins (A) and downregulated proteins (B).

(TIF)

S1 Table. The detail information of all identified peptides.

(XLSX)

S2 Table. The detail information of differential phosphorylated proteins and phosphosites.

(XLSX)

S3 Table. GO enrichment of up- and downregulated phosphoproteins.

(XLSX)

S4 Table. KEGG pathway of differential phosphoproteins.

(XLSX)

S5 Table. Phosphorylation motifs of all sites in proteins of *Glycine max* cv. Tamba.

(XLSX)

S6 Table. Summary of phosphoproteins affected by Al³⁺.

(XLSX)

S7 Table. Node Information of PPI.

(XLSX)

S8 Table. DPPs associated with signal transduction.

(XLSX)

S9 Table. DPPs associated with transcription, translation and posttranslational modification.

(XLSX)

S10 Table. DPPs associated with carbohydrate metabolism.

(XLSX)

S11 Table. DPPs associated with transporters.

(XLSX)

Author Contributions

Conceptualization: Rongrong Han, Yongxiong Yu.

Formal analysis: Rongrong Han, Yunmin Wei.

Investigation: Yonghong Xie.

Methodology: Rongrong Han, Caode Jiang, Yongxiong Yu.

Visualization: Rongrong Han, Lusheng Liu.

Writing – original draft: Rongrong Han.

Writing – review & editing: Caode Jiang, Yongxiong Yu.

References

1. Kochian LV, Piñeros MA, Liu J, Magalhaes JV. Plant adaptation to acid soils: The molecular basis for crop aluminum resistance. *Annu Rev Plant Biol.* 2015; 66(1):571–598. <https://doi.org/10.1093/nar/gkx417>.
2. Fan Y, Ouyang YY, Pan YL, Hong T, Wu CZ, Lin H, et al. Effect of aluminum stress on the absorption and transportation of aluminum and macronutrients in roots and leaves of *Aleurites montana*. *Forest Ecol Manag.* 2020; 458:117813. <https://doi.org/10.1016/j.foreco.2019.117813>.
3. Sade H, Meriga B, Surapu V, Gadi J, Sunita M, Suravajhala P, et al. Toxicity and tolerance of aluminum in plants: tailoring plants to suit to acid soils. *Biomaterials.* 2016; 29(2):187–210. <https://doi.org/10.1007/s10534-016-9910-z> PMID: 26796895
4. Jaskowiak J, Tkaczyk O, Slota M, Kwasniewska J, Szarejko I. Analysis of aluminum toxicity in *Hordeum vulgare* roots with an emphasis on DNA integrity and cell cycle. *PLoS ONE.* 2018; 13(2):e0193156. <https://doi.org/10.1371/journal.pone.0193156> PMID: 29466444
5. Liu JP, Piñeros MA, Kochian LV. The role of aluminum sensing and signaling in plant aluminum resistance. *J Integr Plant Biol.* 2014; 56(3):221–230. <https://doi.org/10.1111/jipb.12162> PMID: 24417891
6. Wang W, Zhao XQ, Chen RF, Dong XY, Lan P, Ma JF, et al. Altered cell wall properties are responsible for ammonium-reduced aluminium accumulation in rice roots. *Plant Cell and Environ.* 2015; 38(7):1382–1390. <https://doi.org/10.1111/pce.12490>.
7. Li JY, Liu JP, Dong DK, Jia XM, McCouch SR, Kochian LV. Natural variation underlies alterations in Nramp aluminum transporter (*NRAT1*) expression and function that play a key role in rice aluminum tolerance. *Proc Natl Acad Sci USA.* 2014; 111(17):6503–6508. <https://doi.org/10.1073/pnas.1318975111> PMID: 24728832
8. Osawa H, Matsumoto H. Possible involvement of protein phosphorylation in aluminum-responsive malate efflux from wheat root apex. *Plant Physiol.* 2001; 126(1):411–420. <https://doi.org/10.1104/pp.126.1.411> PMID: 11351103
9. Jiang CD, Liu LS, Li XF, Han RR, Wei YM, Yu YX. Insights into aluminum-tolerance pathways in *Stylosanthes* as revealed by RNA-Seq analysis. *Sci Rep.* 2018; 8(1):6072. <https://doi.org/10.1038/s41598-018-24536-3> PMID: 29666506
10. Muñoz-Sánchez JA, Chan-May A, Cab-Guillén Y, Hernández-Sotomayor SMT. Effect of salicylic acid on the attenuation of aluminum toxicity in *Coffea arabica* L. suspension cells: A possible protein phosphorylation signaling pathway. *J Inorg Biochem.* 2013; 128:188–195. <https://doi.org/10.1016/j.jinorgbio.2013.07.006> PMID: 23953991
11. Shen H, He LF, Sasaki T, Yamamoto Y, Zheng SJ, Ligaba A, et al. Citrate secretion coupled with the modulation of soybean root tip under aluminum stress. Up-regulation of transcription, translation, and threonine-oriented phosphorylation of plasma membrane H⁺-ATPase. *Plant Physiol.* 2005; 138(1):287–296. <https://doi.org/10.1104/pp.104.058065> PMID: 15834009
12. Wu KH, Xiao SQ, Chen Q, Wang QF, Zhang YN, Li KZ, et al. Changes in the activity and transcription of antioxidant enzymes in response to Al stress in black soybeans. *Plant mol Biol Rep.* 2013; 31(1):141–150. <https://doi.org/10.1007/s11105-012-0487-6>.
13. Min Y, Guo CL, Zhao XL, Wang L, Yu YX, Chen LM. Adenosine 5'-monophosphate decreases citrate exudation and aluminium resistance in Tamba black soybean by inhibiting the interaction between 14-3-3 proteins and plasma membrane H⁺-ATPase. *Plant Growth Regul.* 2018; 84(2):285–292. <https://doi.org/10.1007/s10725-017-0339-3>.

14. Guo CL, Chen Q, Zhao XL, Chen XQ. Al-enhanced expression and interaction of 14-3-3 protein and plasma membrane H⁺-ATPase is related to Al-induced citrate secretion in an Al-resistant black soybean. *Plant Mol Biol Rep*. 2013; 31(4):1012–1024. <https://doi.org/10.1007/s11105-013-0569-0>.
15. Cai SG, Wu DZ, Jabeen Z, Huang YQ, Huang YC, Zhang GP. Genome-wide association analysis of aluminum tolerance in cultivated and Tibetan wild barley. *PLoS ONE*. 2013; 8(7):e69776. <https://doi.org/10.1371/journal.pone.0069776> PMID: 23922796
16. Silva RG, Rosa-Santos TM, Castro França S, Kottapalli P, Kottapalli KR, Zingaretti SM. Microtranscriptome analysis of sugarcane cultivars in response to aluminum stress. *PLoS ONE*. 2019; 14(11):e0217806. <https://doi.org/10.1371/journal.pone.0217806> PMID: 31697688
17. Zhou DW, Yang Y, Zhang JB, Jiang F, Craft E, Thannhauser TW, et al. Quantitative iTRAQ proteomics revealed possible roles for antioxidant proteins in sorghum aluminum tolerance. *Front plant sci*. 2017; 7:2043. <https://doi.org/10.3389/fpls.2016.02043> PMID: 28119720
18. Sun HG, Xia BL, Wang X, Gao F, Zhou YJ. Quantitative phosphoproteomic analysis provides insight into the response to short-term drought stress in *Ammopiptanthus mongolicus* roots. *Int J Mol Sci*. 2017; 18(10):2158. <https://doi.org/10.3390/ijms18102158>.
19. Hou YX, Qiu JH, Tong XH, Wei XJ, Nallamilli BR, Wu WH, et al. A comprehensive quantitative phosphoproteome analysis of rice in response to bacterial blight. *BMC Plant Biol*. 2015; 15(1):163. <https://doi.org/10.1186/s12870-015-0541-2>.
20. Wang N, Zhu TQ, Lu N, Wang Z, Yang GY, Qu GY, et al. Quantitative phosphoproteomic and physiological analyses provide insights into the formation of the variegated leaf in *Catalpa fargesii*. *Int J Mol Sci*. 2019; 20(8):1895. <https://doi.org/10.3390/ijms20081895>.
21. Huang SC, Baloch SK, Shu YJ, Ali M, Baloch AW, Rajper AA, et al. Identification and analysis of differentially expressed genes associated with aluminum response in two soybean cultivars by cDNA-RAPD. *Pak J Bot*. 2015; 47(2):711–715.
22. Zhao ZQ, Ma JF, Sato K, Takeda K. Differential Al resistance and citrate secretion in barley (*Hordeum vulgare* L.). *Planta*. 2003; 217(5):794–800. <https://doi.org/10.1007/s00425-003-1043-2> PMID: 12734756
23. Chen MY, Zhu AJ, Storey KB. Comparative phosphoproteomic analysis of intestinal phosphorylated proteins in active versus aestivating sea cucumbers. *J Proteomics*. 2015; 135:141–150. <https://doi.org/10.1016/j.jprot.2015.09.016> PMID: 26385000
24. Eticha D, Zahn M, Bremer M, Yang ZB, Rangel AF, Rao IM, et al. Transcriptomic analysis reveals differential gene expression in response to aluminium in common bean (*Phaseolus vulgaris*) genotypes. *Annals bot*. 2010; 105(7):1119–1128. <https://doi.org/10.1093/aob/mcq049>.
25. Wang HH, Zhang YY, Hou JJ, Liu WW, Liang WH. Nitric oxide mediates aluminum-induced citrate secretion through regulating the metabolism and transport of citrate in soybean roots. *Plant soil*. 2019; 435(1–2):127–42. <https://doi.org/10.1007/s11104-018-3879-z>.
26. Li WH, Du J, Feng HM, Wu Q, Xu GH, Shabala S, et al. Function of NHX-type transporters in improving rice tolerance to aluminum stress and soil acidity. *Planta*. 2020; 251(3):71. <https://doi.org/10.1007/s00425-020-03361-x> PMID: 32108903
27. Melo JO, Martins LG, Barros BA, Pimenta MR, Lana UG, Duarte CE, et al. Repeat variants for the SbMATE transporter protect sorghum roots from aluminum toxicity by transcriptional interplay in *cis* and *trans*. *Proc Natl Acad Sci USA*. 2019; 116(1):313–318. <https://doi.org/10.1073/pnas.1808400115> PMID: 30545913
28. Inostroza-Blancheteau C, Rengel Z, Alberdi M, de la Luz Mora M, Aquea F, Arce-Johnson P, et al. Molecular and physiological strategies to increase aluminum resistance in plants. *Mol Biol Rep*. 2012; 39(3):2069–2079. <https://doi.org/10.1007/s11033-011-0954-4> PMID: 21660471
29. Zhou ZH, Fu XD. Regulation of splicing by SR proteins and SR protein-specific kinases. *Chromosoma*. 2013; 122(3):191–207. <https://doi.org/10.1007/s00412-013-0407-z> PMID: 23525660
30. Reinbothe C, Pollmann S, Reinbothe S. Singlet oxygen signaling links photosynthesis to translation and plant growth. *Trends Plant Sci*. 2010; 15(9):499–506. <https://doi.org/10.1016/j.tplants.2010.05.011> PMID: 20580304
31. Cardano M, Zasso J, Ruggiero L, Giacomo GD, Marcatili M, Cremona O, et al. Epsins regulate mouse embryonic stem cell exit from pluripotency and neural commitment by controlling notch activation. *Stem cells Int*. 2019; 2019. <https://doi.org/10.1155/2019/4084351>.
32. Yu JH, Li YR, Zou F, Xu SM, Liu PS. Phosphorylation and function of DGAT1 in skeletal muscle cells. *Biophys Rep*. 2015; 1(1):41–50. <https://doi.org/10.1007/s41048-015-0004-1>.
33. Gao AL, Wu QY, Zhang Y, Miao YC, Song CP. *Arabidopsis* calcium-dependent protein kinase CPK28 is potentially involved in the response to osmotic stress. *Chin sci bull*. 2014; 59(11):1113–1122. <https://doi.org/10.1007/s11434-013-0062-z>.

34. Mi JK, Go YS, Lee SB, Kim YS, Shin JS, Min MK, et al. Seed-expressed casein kinase I acts as a positive regulator of the *SeFAD2* promoter via phosphorylation of the SebHLH transcription factor. *Plant Mol Biol*. 2010; 73(4–5):425–437. <https://doi.org/10.1007/s11103-010-9630-7> PMID: 20349267
35. Li GZ, Wang ZQ, Yokosho K, Ding B, Fan W, Gong QQ, et al. Transcription factor WRKY22 promotes aluminum tolerance via activation of *OsFRDL4* expression and enhancement of citrate secretion in rice (*Oryza sativa*). *New Phytol*. 2018; 219(1):149–162. <https://doi.org/10.1111/nph.15143>.
36. Zhang X, Li L, Yang C, Cheng Y, Han ZZ, Cai ZD, et al. GsMAS1 encoding a MADS-box transcription factor enhances the tolerance to aluminum stress in *Arabidopsis thaliana*. *Int J Mol Sci*, 2020, 21(6):2004. <https://doi.org/10.3390/ijms21062004>.
37. Jin JF, Wang ZQ, He QY, Wang JY, Li PF, Xu JM, et al. Genome-wide identification and expression analysis of the NAC transcription factor family in tomato (*Solanum lycopersicum*) during aluminum stress. *BMC Genomics*, 2020; 21:288. <https://doi.org/10.1186/s12864-020-6689-7> PMID: 32264854
38. Escobar-Sepúlveda HF, Trejo-Téllez LI, García-Morales S, Gómez-Merino FC. Expression patterns and promoter analyses of aluminum-responsive NAC genes suggest a possible growth regulation of rice mediated by aluminum, hormones and NAC transcription factors. *PLoS ONE*. 2017; 12(10): e0186084. <https://doi.org/10.1371/journal.pone.0186084> PMID: 29023561
39. Xu LM, Liu C, Cui BM, Wang N, Zhao Z, Zhou LN, et al. Transcriptomic responses to aluminum (Al) stress in maize. *J Integr Agric*. 2018; 17(9):1946–1958. [https://doi.org/10.1016/S2095-3119\(17\)61832-X](https://doi.org/10.1016/S2095-3119(17)61832-X).
40. Pi EX, Xu J, Li HH, Fan W, Zhu CM, Zhang TY, et al. Enhanced salt tolerance of rhizobia-inoculated soybean correlates with decreased phosphorylation of the transcription factor GmMYB183 and altered flavonoid biosynthesis. *Mol Cell Proteomics*. 2019; 18(11):2225–2243. <https://doi.org/10.1074/mcp.RA119.001704> PMID: 31467032
41. Hoang MHT, Nguyen XC, Lee K, Kwon YS, Pham HTT, Park HC, et al. Phosphorylation by AtMPK6 is required for the biological function of AtMYB41 in *Arabidopsis*. *Biochem Bioph Res Co*. 2012; 422(1):181–186. <https://doi.org/10.1016/j.bbrc.2012.04.137>.
42. Liu XM, Nguyen XC, Kim KE, Han HJ, Yoo J, Lee K, et al. Phosphorylation of the zinc finger transcriptional regulator ZAT6 by MPK6 regulates *Arabidopsis* seed germination under salt and osmotic stress. *Biochem Bioph Res Co*. 2013; 430(3):1054–1059. <https://doi.org/10.1016/j.bbrc.2012.12.039>.
43. Jia YX, Ding YL, Shi YT, Zhang XY, Gong ZZ, Yang SH. The *cbfs* triple mutants reveal the essential functions of CBFs in cold acclimation and allow the definition of CBF regulons in *Arabidopsis*. *New Phytol*. 2016; 212(2):345–353. <https://doi.org/10.1111/nph.14088>.
44. Kim SH, Kim HS, Bahk S, An J, Yoo Y, Kim JY, et al. Phosphorylation of the transcriptional repressor MYB15 by mitogen-activated protein kinase 6 is required for freezing tolerance in *Arabidopsis*. *Nucleic Acids Res*. 2017; 45(11):6613–6627. <https://doi.org/10.1093/nar/gkx417> PMID: 28510716
45. Furihata T, Maruyama K, Fujita Y, Umezawa T, Yoshida R, Shinozaki K, et al. Abscisic acid-dependent multisite phosphorylation regulates the activity of a transcription activator AREB1. *Proc Natl Acad Sci USA*. 2006; 103(6):1988–1993. <https://doi.org/10.1073/pnas.0505667103> PMID: 16446457
46. Iuchi S, Kobayashi Y, Koyama H, Kobayashi M. STOP1, a Cys2/His2 type zinc-finger protein, plays critical role in acid soil tolerance in *Arabidopsis*. *Plant signaling & behavior*. 2008; 3(2):128–130. <https://doi.org/10.4161/psb.3.2.5037>.
47. Hardin SC, Huber SC. Proteasome activity and the post-translational control of sucrose synthase stability in maize leaves. *Plant Physiol Biochem*. 2004; 42(3):197–208. <https://doi.org/10.1016/j.plaphy.2003.12.004> PMID: 15051043
48. Chen L, Li Z, Li X, Chen J, Everaert N, Zhang DQ. The effect of sarcoplasmic protein phosphorylation on glycolysis in postmortem ovine muscle. *Int J Food Sci Technol*. 2018; 53(12):2714–2722. <https://doi.org/10.1111/ijfs.13882>.
49. Liu N, You JF, Shi WL, Liu W, Yang ZM. Salicylic acid involved in the process of aluminum induced citrate exudation in *Glycine max* L. *Plant Soil*. 2012; 352(1–2):85–97. <https://doi.org/10.1007/s11104-011-0981-x>.
50. Walker RP, Paoletti A, Leegood RC, Famiani F. Phosphorylation of phosphoenolpyruvate carboxylase (PEPCK) and phosphoenolpyruvate carboxylase (PEPC) in the flesh of fruits. *Plant Physiol Biochem*. 2016; 108:323–327. <https://doi.org/10.1016/j.plaphy.2016.07.021> PMID: 27497301
51. Chao Q, Liu XY, Mei YC, Gao ZF, Chen YB, Qian CR, et al. Light-regulated phosphorylation of maize phosphoenolpyruvate carboxylase plays a vital role in its activity. *Plant Mol Biol*. 2014; 85(1):95–105. <https://doi.org/10.1007/s11103-014-0171-3>.